ACS OMEGA

Open Access

http://pubs.acs.org/journal/acsodf

Article

Highly Macroporous Polyimide with Chemical Versatility Prepared from Poly(amic acid) Salt-Stabilized High Internal Phase Emulsion Template

Jongmin Park,[#] Sunkyu Kim,[#] Jeonguk Hwang, Jun Ha Choi, Yujin So, Sarang Park, Min Jae Ko, Jong Chan Won, Jungdon Suk, Mihye Wu,* and Yun Ho Kim*

Cite This: *ACS Omega* 2024, 9, 15222−15231

Read Online

ACCESS | Metrics & More | Article Recommendations | Supporting Information

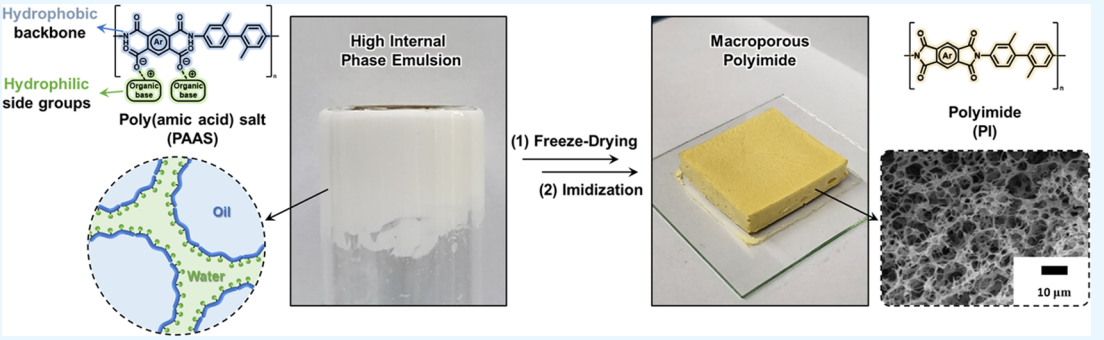

ABSTRACT: Macroporous polymers have gained significant attention due to their unique mass transport and size-selective properties. In this study, we focused on Polyimide (PI), a high-performance polymer, as an ideal candidate for macroporous structures. Despite various attempts to create macroporous PI (Macro PI) using emulsion templates, challenges remained, including limited chemical diversity and poor control over pore size and porosity. To address these issues, we systematically investigated the role of poly(amic acid) salt (PAAS) polymers as macrosurfactants and matrices. By designing 12 different PAAS polymers with diverse chemical structures, we achieved stable high internal phase emulsions (HIPEs) with >80 vol % internal volume. The resulting Macro PIs exhibited exceptional porosity (>99 vol %) after thermal imidization. We explored the structure−property relationships of these Macro PIs, emphasizing the importance of controlling pore size distribution. Furthermore, our study demonstrated the utility of these Macro PIs as separators in Li-metal batteries, providing stable charging−discharging cycles. Our findings not only enhance the understanding of emulsion-based macroporous polymers but also pave the way for their applications in advanced energy storage systems and beyond.

INTRODUCTION

Macroporous polymers are porous polymers containing porous structures of >50 nm, as classified by the International Union of Pure and Applied Chemistry (IUPAC).[1−5] Their high porosities, large surface areas, and well-defined pore sizes provide mass transport and size-selective properties, which render them invaluable for use in various applications, including thermal and mechanical insulation, material separation, and catalytic support. Several methods of producing macroporous polymers have been proposed, such as polymer blending, nonsolvent-induced phase separation (NIPS),[6−9] powder foaming,[10,11] freeze-drying,[12,13] and soft-template methods.[14−19] The resulting porous polymers exhibit different morphologies and porosities, which alter their mechanical properties. In addition, the chemical structure of the polymer matrix also affects the mechanical strength and thermal stability of the porous polymer. Therefore, the design of macroporous polymers should consider the synthetic method and polymer species to obtain the desired morphologies, controllable pore sizes, and high porosities with sufficient physical stability.

Polyimide (PI) is a high-performance polymer with excellent thermal stability, mechanical strength, corrosion resistance, and hydrolytic stability at elevated temperatures.[20,21] These properties render it an ideal candidate for application in a macroporous polymer for use in harsh environments because its excellent physical strength ensures the structural stability of the porous polymer. The synthesis of macroporous PI (Macro

Received: December 2, 2023
Revised: February 28, 2024
Accepted: March 6, 2024
Published: March 22, 2024

PI) has been proposed by utilizing the strategies to produce the porous structure.[3−5,7−13,15,16] These Macro PIs possess structural stability under a wide range of temperature changes and external stress, which makes it possible to be utilized in applications, including batteries,[22−24] telecommunication,[25] thermal insulation,[26,27] and electromagnetic interference.[28,29] Although various types of Macro PIs have been proposed, a synthetic strategy for use in yielding a continuous porous morphology and high porosity (>99 vol %) is still required to maximize the advantages of the porous structure.

To address these challenges, the emulsion template method has been proposed as a promising approach for use in producing Macro PI. A high internal phase emulsion (HIPE), which is a special type of emulsion, provides a high porosity (∼90 vol %) and bicontinuous porous morphology owing to its special feature, i.e., >74 vol % of the internal volume is covered by a continuous external phase.[14−17] The Macro PIs prepared using HIPE templates are generally formed by stabilizing the interfaces between the immiscible liquids with amphiphilic molecules or nanoparticles.[30−35] To obtain a porous polymeric monolith using HIPE, the structure is fixed by freezing or cross-linking of the external phase, followed by washing or drying of the internal phase. However, the emulsifiers on the polymer surfaces are not completely eliminated, causing the plasticization of the polymer matrix and deformation of the porous structure.[36,37] Therefore, the remaining emulsifiers should be removed via an additional process to avoid weakening of the mechanical and thermal properties of the resulting porous polymer. Furthermore, the low solubility of PI constrains the chemical diversity of the polymer because it should be dissolved in the solution to be applied in an emulsion template.

As an alternative approach, our group suggested the use of the poly(amic acid) salt (PAAS) polymer as the macrosurfactant of an oil-in-water (o/w) HIPE.[38,39] The water-soluble PAAS polymer displays an intrinsic amphiphilicity due to its chemical structure consisting of the aromatic polymer backbone conjugated with protonated organic bases.[40−43] The PAAS polymer poly(3,3′,4,4′-biphenyltetracarboxylic dianhydride-*co*-*m*-tolidine) conjugated with *N*,*N*′-dimethylethanolamine (BPDA-mTB/DMEA) exhibits a sufficient amphiphilicity to form a (o/w) HIPE having an internal volume of >80 vol %, even at a low PAAS mass content (∼3 wt %). Furthermore, porous PI was successfully obtained by converting the PAAS to PI scaffold via a well-known thermal imidization process.[39−42,44] The Macro PI obtained via our emulsion template method is thermally stable with elastic properties and is useful as a solar desalination membrane and separator in Li-metal batteries. Nevertheless, the limitations of the PAAS-mediated emulsion template method remain, including (1) the limited combination in chemical diversity of the polymer backbone and organic base, (2) a lack of understanding of the design of the PAAS polymer for use in the emulsion, and (3) the control of the pore size and porosity of the resulting polymer.

To this end, we systematically investigated the role of the PAAS polymer as a macrosurfactant and matrix. A critical factor for an emulsifier is the hydrophobic−hydrophilic balance, which is derived from changes in the chemical structure. To explore this, we designed 12 different PAAS polymers comprising three polymer backbones and four organic bases. Rheological analyses of the PAAS-mediated HIPEs confirmed the effect of the chemical structure on the stability of the emulsion. We also fabricated Macro PIs with porosities of >99 vol % via thermal imidization using stable HIPEs to observe their porous morphologies and physical properties. Thus, we analyzed the structure−property relationships of Macro PIs and the significance of controlling the pore size distribution. Finally, we investigated the utilization of our polymer as a separator for use in Li-metal batteries to yield stable charging−discharging. Our results suggest that the PAAS polymer deserves the interfacial activity as well as the mechanical stability for the highly porous macroporous polymer by being converted to the robust polyimide polymer via the thermal process. Therefore, the use of PAAS polymer as the macrosurfactant provides us with an efficient methodology to prepare the physically robust polymeric scaffold by avoiding the use of additional emulsifiers.

EXPERIMENTAL SECTION

Materials. Unless otherwise stated, the chemicals were used as received. Pyromellitic dianhydride (PMDA), 3,3′,4,4′-biphenyltetracarboxylic dianhydride (BPDA), and 4,4′-(hexafluoroisopropylidene)diphthalic anhydride (6FDA) were kindly provided by PI Advanced Materials (Seoul, Republic of Korea). The anhydrides were dried under vacuum at 180 °C for 24 h prior to use. *m*-Tolidine (mTB) was purchased from Changzhou Sunlight Pharmaceutical (Changzhou, China), and organic bases 4-dimethylaminopyridine (DMAP, 99%), triethylamine (TEA, 99.5%), 1,2-dimethylimidazole (DMIZ, 97%), and *N*,*N*-dimethylethanolamine (DMEA, 99.5%) were purchased from Merck (Darmstadt, Germany). *N*,*N*-Dimethylacetamide (DMAc, 99%) was purchased from Junsei Chemical (Tokyo, Japan), and deionized H_2O was purified prior to use using an H_2O purification system (UP DLX) from Human Science (Hanam, Republic of Korea).

Methods. ^{1}H nuclear magnetic resonance (^{1}H NMR) spectroscopy was performed using an Avance 500 MHz spectrometer (Bruker, Billerica, MA) with the residual solvent signal as an internal standard. Fourier transform infrared (FT-IR) spectroscopy was conducted using an α-P spectrophotometer (Bruker) in the range 650−4000 cm^{-1} under ambient conditions. Size exclusion chromatography (SEC) was conducted in *N*-methyl-2-pyrrolidone with 0.02 M H_3PO_4 and 0.02 M LiBr at 50 °C with a flow rate of 0.8 mL min^{-1} using a Shodex (Showa Denko, Tokyo, Japan). The molar masses of the polymers were calculated relative to linear polystyrene standards purchased from Agilent Technologies (CA). The instrument was equipped with three poly(hydroxy methacrylate) columns (multipore) with molar masses in the range of 200−20 000 000 g mol^{-1}. Thermogravimetric analysis (TGA) was performed using a TGA Q500 (TA Instruments, New Castle, DE) in the range of 25−800 °C at a heating rate of 10 °C min^{-1}, and compression studies were performed using a 4482 universal testing system (Instron, Norwood, MA). The rheological properties were measured using a rheometer (MCR 302, Anton Paar, Graz, Austria) with parallel plate geometry with a 25 mm diameter, and the loaded gap between the plates was 1.0 mm. In the frequency sweep mode, the shear moduli were measured at a fixed strain amplitude (10%) with angular frequencies from 0.1 to 100 rad s^{-1}. In the amplitude sweep mode, the shear moduli were measured at a fixed frequency (1.0 rad s^{-1}) with strain amplitudes from 0.01 to 100% (0.0001−1). The porosity of the resulting porous polymer was determined by utilizing the equation: porosity (p) = 1 − (ρ_{film}/$\rho_{Macro\ PI}$), where ρ_{film} = bulk density of the polyimide film with

https://doi.org/10.1021/acsomega.3c09640
ACS Omega 2024, 9, 15222−15231

Table 1. Pore Characteristics and Physical Properties of Macro PIs

		pore characteristics		physical properties	
polymer backbone	organic base	D_{avg} (μm)[a]	porosity (%)[b]	$T_{d,5\%}$ (°C)	compression modulus (kPa)[c]
PMDA-mTB	DMAP	16.7 ± 9.8	99.54	468	11.6
	TEA	10.2 ± 4.6	99.58	530	25.7
	DMIZ	14.2 ± 9.6	99.50	519	15.6
	DMEA	15.3 ± 9.3	99.56	500	13.6
BPDA-mTB	DMAP	24.8 ± 16.3	99.40	508	23.6
	TEA	13.4 ± 6.7	99.54	532	47.9
	DMIZ	13.5 ± 8.0	99.48	516	42.2
	DMEA	21.0 ± 10.9	99.56	521	26.6
6FDA-mTB	TEA	11.3 ± 7.1	99.34	465	22.5
	DMIZ	6.6 ± 3.9	99.38	465	15.2
	DMEA	21.4 ± 12.6	99.38	472	27.7

[a]The average pore diameter (D_{avg}) was determined using an SEM image. [b]The porosity was determined based on the density. [c]The modulus was obtained from the stress−strain curve measured during the compression study.

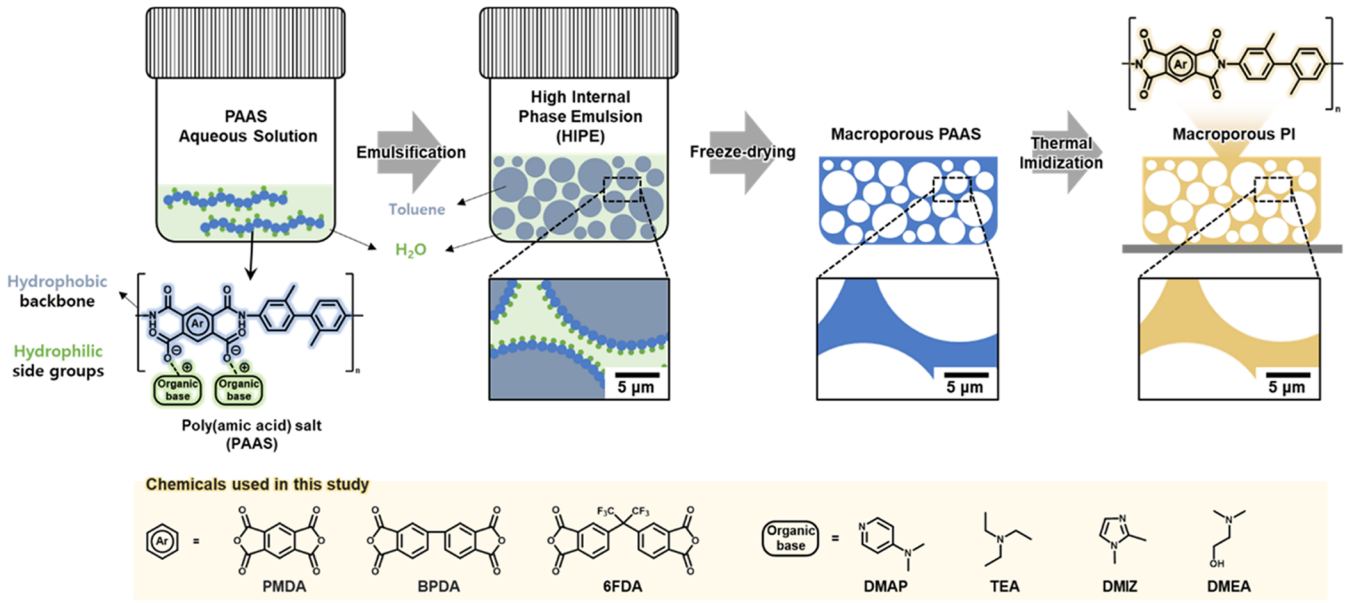

Figure 1. Schematic of the synthetic procedure used in preparing macroporous polyimide (Macro PI) via the emulsion template method using the aqueous poly(amic acid) salt (PAAS) polymer solution. PMDA, pyromellitic dianhydride; BPDA, 3,3′,4,4′-biphenyltetracarboxylic dianhydride; 6FDA, 4,4′-(hexafluoroisopropylidene)diphthalic anhydride; DMAP, 4-dimethylaminopyridine; TEA, triethylamine; DMIZ, 1,2-dimethylimidazole; and DMEA, *N,N*-dimethylethanolamine.

identical chemical structure; $\rho_{Macro\ PI}$ = density of the Macro PI obtained in this study. The density of polymer film and Macro PI was determined by measuring the weight with analytical balance from Mettler Toledo (OH) and height of 1 × 1 cm^2 sized polymers. The measurement was repeated three times for each sample, and the averaged results are summarized in Table 1. Nitrogen adsorption isotherms were obtained on an ASAP 2420 analyzer from Micromeritics (GA) at the temperature of liquid nitrogen (77.3 K). Specific surface area (S_{N_2}) was estimated by multipoint Brunauer−Emmett−Teller (BET) analysis (between $0.05 < P/P_0 < 0.25$).[45]

Synthesis of Poly(amic acid) (PAA). PAA polymers were synthesized using identical procedures, and BPDA-mTB is used as an example. mTB (2.4332 g, 11.4611 mmol) was dissolved in 55.7 mL of DMAc under N_2 gas, and BPDA (3.3835 g, 11.4611 mmol) was added to the mTB solution, which was stirred at 0 °C for 4 h. The PAA was purified by precipitating the crude solution in acetone, and the generated polymer was collected and dried under a vacuum at 40 °C for 24 h. Identical procedures were used to prepare the PMDA-mTB and 6FDA-mTB polymer precursors, and the ^{1}H NMR spectra are shown in Figure S2.

Synthesis of Poly(amic acid) Salt (PAAS). PAAS polymers were prepared by neutralizing the PAA polymers with an organic base under aqueous conditions using identical procedures, and BPDA-mTB/DMIZ is used as an example. The BPDA-mTB polymer (1.0000 g) was placed in a 120 mL vial with 32.3 g of deionized H_2O. To proceed with the acid−base reaction, DMIZ (0.3796 g, 3.9486 mmol) was added to the aqueous solution. The reaction mixture was stirred at room temperature (RT) for 6 h, and thus, a transparent aqueous solution of PAAS was obtained. Identical procedures were applied in preparing the other 11 types of PAAS polymer precursors, and their details are shown in Figures S2 and S5 and Table S1.

Synthesis of the Macro PIs. The synthesis of a Macro PI, which was derived from 10 vol % of the aqueous phase containing 3 wt % of BPDA-mTB/DMIZ and 90 vol % of the

https://doi.org/10.1021/acsomega.3c09640
ACS Omega 2024, 9, 15222−15231

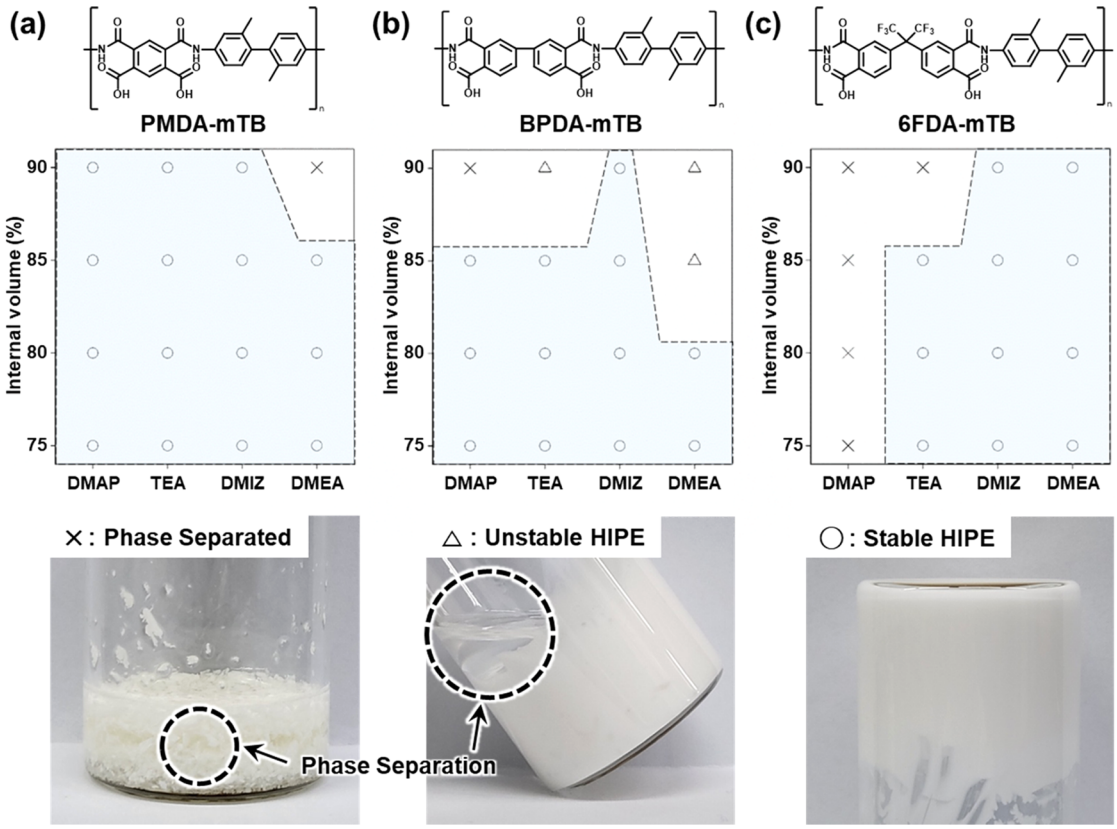

Figure 2. Phase diagram of stable high internal phase emulsion (HIPE) formation using 3 wt % of the poly(amic acid) salt solutions. The images represent the symbols in the phase diagrams—○: stable HIPE, △: unstable HIPE (phase separation within 30 min), and ×: phase separation into a two-phase state.

oil phase (toluene), is used as an example. An aqueous solution containing 3 wt % BPDA-mTB/DMIZ was placed in a 120 mL vial and used as the external phase. Toluene was added dropwise to the aqueous phase with mixing using a homogenizer to form the HIPE. The internal volume was varied from 75 to 90 vol % to evaluate the stability of the resulting emulsion. The HIPE was then poured onto a glass substrate equipped with a 40 × 40 × 10 mm^3 Si mold to form a rectangular shape. The shaped HIPE was placed in a freeze-dryer (MP-9005, Mareuda, Gwangju, Republic of Korea) at −40 °C for 30 min and then dried under vacuum for 24 h. The obtained white polymer was converted to the Macro PI via thermal imidization by increasing the temperature from RT to 350 °C having 50 °C intervals with a time of 30 min at each stage. The conversion of PAAS to PI in the polymer matrix was observed by using FT-IR spectroscopy, and Macro PIs with a wide range of compositions could be prepared. The porosity of the Macro PI was tuned by varying the internal volume from 75 to 90 vol %, and PIs with different chemical structures could also be used to prepare Macro PIs by varying the chemical structure of PAAS.

Electrochemical Measurements. CR2032 coin cells were fabricated using Li metal and Celgard 2400 as the anodes and separators, respectively, and an electrolyte consisting of 1 M $LiPF_6$ dissolved in 1:1 ethylene carbonate/dimethyl carbonate (v/v). The electrolyte contained 10 wt % fluoroethylene carbonate and 2 wt % vinylene carbonate as additives, and the entire cell-assembly process was performed in an Ar-filled glovebox. To evaluate the electrochemical performances, Li/Cu cells were fabricated, and galvanostatic charge−discharge curves were measured using a battery cycler (WBCS3000, WonAtech, Seoul, Republic of Korea) in a constant current mode. During the evaluation, a constant current density of 5.0 mA cm^{-2} was applied, aiming to realize a specific capacity of 3.0 mAh cm^{-2}.

RESULTS AND DISCUSSION

The process used in synthesizing Macro PI using PAAS as the emulsifier in HIPE is shown in Figure 1. Because the chemical structure of PAAS polymer consists of a hydrophobic polymer backbone and hydrophilic organic base, the PAAS polymer has intrinsic amphiphilic properties. This amphiphilicity of the polymer provides sufficient interfacial stability to form an oil-in-water (o/w) emulsion. We confirmed that a maximum of 90 vol % of the internal phase was achieved by using toluene and water as internal and external phase mediums, indicating that paste-like HIPE was successfully prepared. Freeze-drying at −40 °C for 24 h is conducted to yield a HIPE with a continuous 3D porous structure, fixing the external phase and removing the solvents to produce macroporous PAAS. Subsequently, the PAAS scaffold undergoes successful thermal imidization to convert it to PI while retaining the porous structure of the precursor.

We prepared 12 distinct types of PAAS polymers to verify the effect of the chemical structure on emulsification. The polymers are synthesized via a two-step procedure comprising the synthesis of PAA and a salt-forming process, as shown in Figure S1 (see the Experimental Section for details). *m*-Tolidine (*m*TB) is utilized as the diamine, and three different dianhydrides, i.e., pyromellitic dianhydride (PMDA), 3,3′,4,4′-

https://doi.org/10.1021/acsomega.3c09640
ACS Omega 2024, 9, 15222−15231

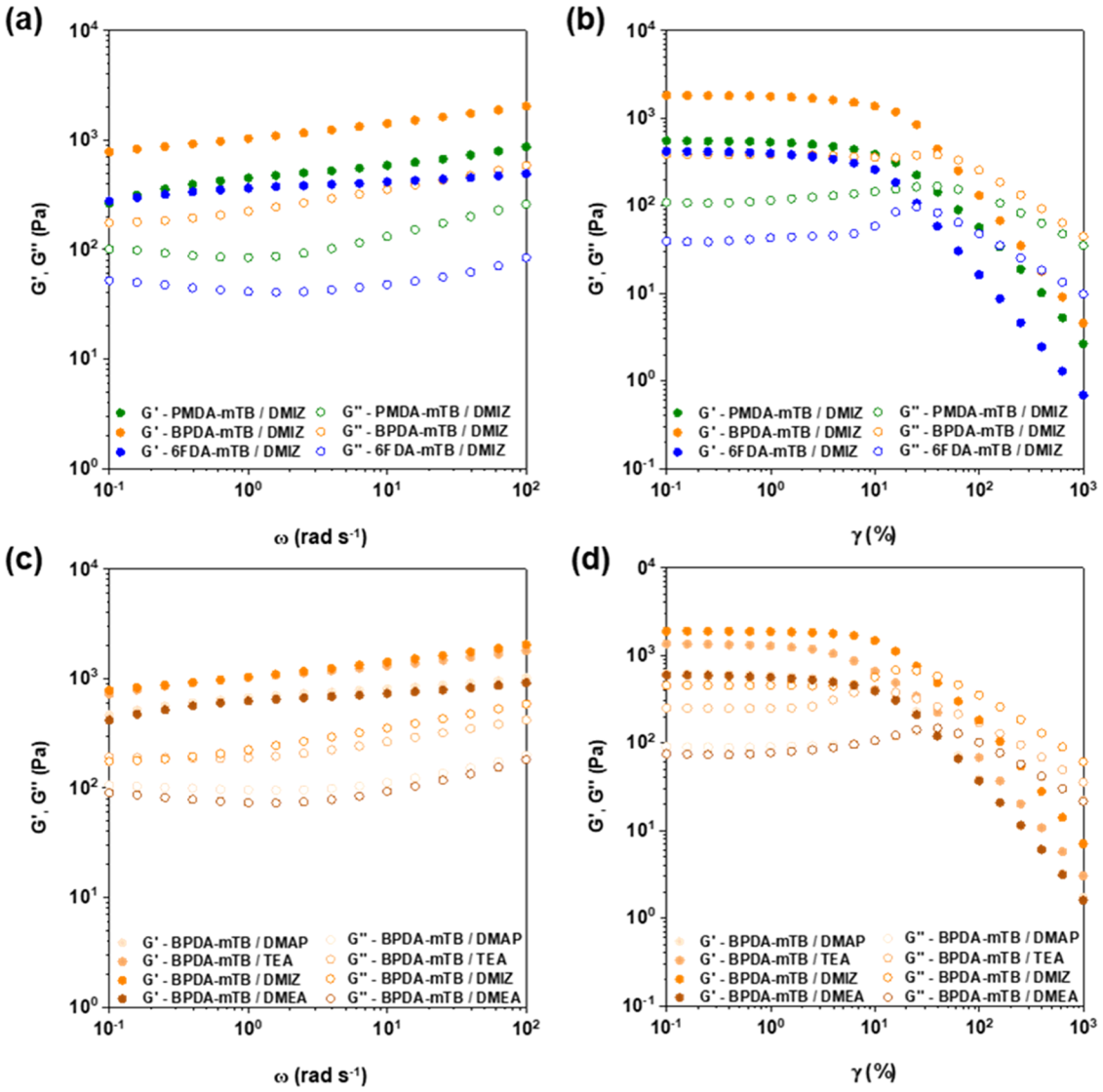

Figure 3. Oscillatory measurements of the poly(amic acid) salt-stabilized high internal phase emulsions in the (a, c) frequency (γ = 0.1−1000%, ω = 1 rad s^{-1}) and (b, d) amplitude sweep modes (γ = 10%, ω = 0.1−100 rad s^{-1}).

biphenyltetracarboxylic dianhydride (BPDA), and 4,4′-(hexafluoroisopropylidene)diphthalic anhydride (6FDA), are used. The PAAs are synthesized by polymerization via nucleophilic addition reactions between the dianhydride and diamine, and the chemical structures of the PAA polymers were verified by using ^{1}H NMR spectroscopy (Figure S2). As the salt-forming agents used in preparing the PAAS polymers, we used tertiary amines, i.e., 4-dimethylaminopyridine (DMAP), triethylamine (TEA), 1,2-dimethylimidazole (DMIZ), and *N*,*N*-dimethylethanolamine (DMEA), which exhibit different solubilities under aqueous conditions. By conjugating the polymer backbones with organic bases under the aqueous condition, we successfully prepared 11 types of aqueous PAAS solutions. It must be noted that the 6FDA-mTB/DMAP was not prepared due to the full solubility of the resulting polymer in water. We named the resulting polymers based on their monomers and organic bases, for example, PAAS with a PMDA-mTB backbone conjugated with DMIZ is denoted PMDA-mTB/DMIZ.

The chemical structures of the resulting PAAs and PAASs were characterized by using ^{1}H NMR spectroscopy and SEC (Figures S2−S6). As a representative example, the ^{1}H NMR spectrum of PMDA-mTB is shown in Figure S2 (green). The characteristic signals observed at 7.00−9.00, 10.53, and 13.27 ppm correspond to protons from the aromatic ring, amide bonds, and carboxylic acid. The chemical structure of BPDA-mTB and 6FDA-mTB was also identified from the ^{1}H NMR spectra, suggesting that the PAA polymers are synthesized. By using PAA polymers as the precursor, the PAAS polymers were synthesized via the salt-forming process using water as a solvent. As a result, the signals representing the carboxylic acids were diminished, and signals from the organic bases appeared, while the aromatic protons from the polymer backbone were nearly intact (Figures S3−S5). Based on the SEC traces of the PMDA-mTB series (Figure S6a and Table S1), the PAAS traces display unimodal distributions without low-molar-mass species at high elution times, indicating that the conjugations of the salts at the carboxyl groups proceed uniformly for all organic bases. BPDA-mTB and PMDA-mTB also exhibit identical tendencies with deviations in molar mass and dispersity ($Đ$). Hence, the PAASs are successfully synthesized via the proposed synthetic procedure.

https://doi.org/10.1021/acsomega.3c09640
ACS Omega 2024, 9, 15222−15231

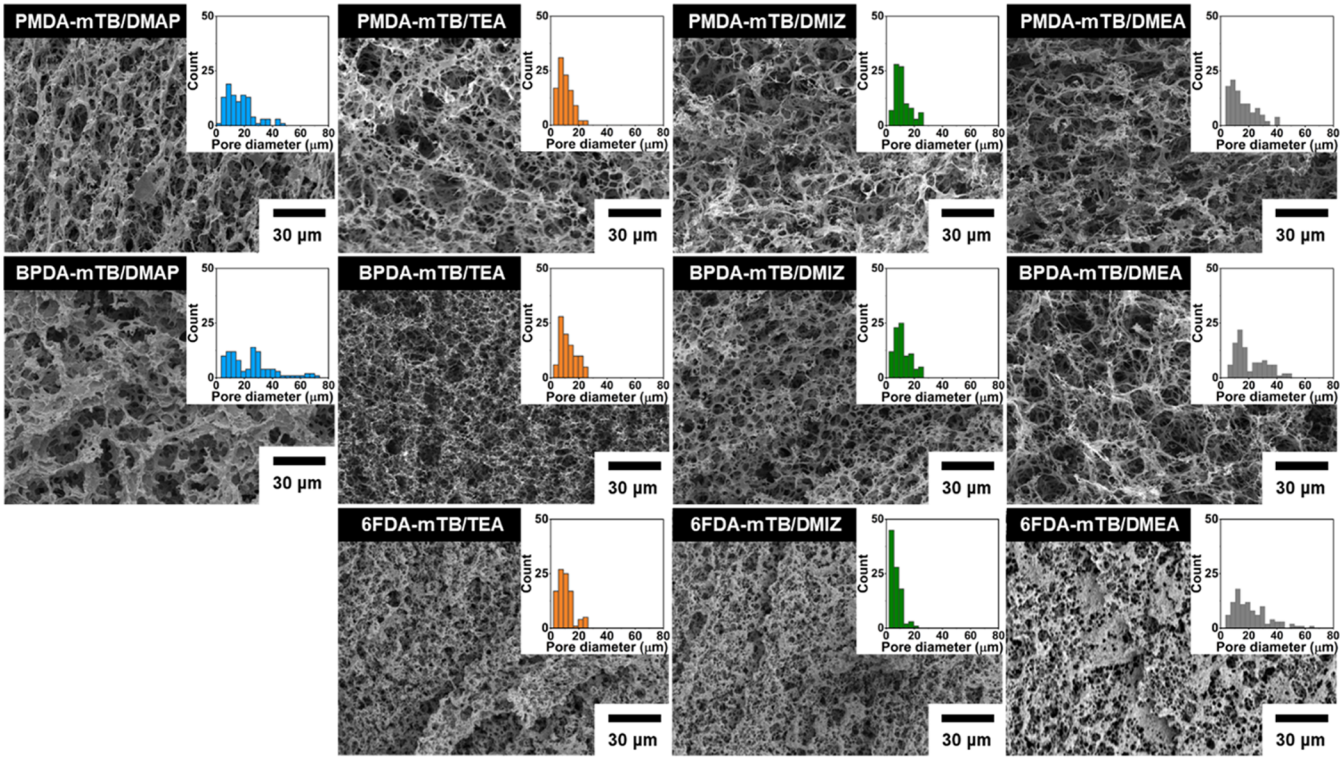

Figure 4. Pore characteristics of the macroporous polyimides, as observed via scanning electron microscopy, and their pore size distributions (insets).

We investigated the stability of the HIPE based on the chemical structure of the PAAS backbone and the tethered organic bases. HIPEs with varying volume fractions of their internal phases from 75 to 90 vol % were prepared using PAAS polymers as the only emulsifiers in the emulsion templates. The prepared HIPEs were monitored for 30 min under ambient conditions to determine their stabilities, as shown in Figure 2. The PAASs with PMDA-mTB backbones exhibit stable HIPE states over a wide range of internal volumes and changes in the organic base. Except for that containing DMEA, the PMDA-mTB-based PAASs yield stable HIPEs at internal volumes of 90 vol %. The optical microscopy image of HIPEs from PMDA-mTB series supported the fact that the PAAS polymers were well-stabilized in the toluene-water interface (Figure S7). The micrograph clearly shows the emulsion structure consists of the internal toluene droplets (light part, 85 vol %) covered by the external water phase (dark part, 15 vol %). The average HIPE droplet sizes were 4.1, 5.5, 8.2, and 9.4 μm for PMDA-mTB/TEA, PMDA-mTB/DMIZ, PMDA-mTB/DMAP, and PMD-mTB/DMEA, respectively. The 6FDA-mTB backbone also exhibits good emulsion stability when it is conjugated with DMIZ and DMEA. When the polymer backbone is BPDA-mTB, the polymer with DMIZ is the sole combination that yields a stable HIPE at an internal volume of 90 vol %, whereas the polymers with the other organic bases undergo phase separation within the observation time. At an internal volume of 80 vol %, the BPDA-mTB-base polymer solutions yield stable HIPEs, regardless of the organic base. Additionally, DMIZ-conjugated PAAS always yields a stable HIPE at an internal volume of 90 vol %, regardless of the polymer backbone.

Because structural fixation proceeds via freeze-drying, the formation of a stable HIPE with sufficient mechanical properties is necessary to prevent deformation. Oscillatory shear measurements of the HIPEs with internal volumes of 80 vol % were performed to observe the dependences of the moduli and yield stress on the chemical structure of the PAAS polymer (Figure 3). The resulting HIPEs display a stronger storage modulus (G') than loss modulus (G''), suggesting that they are viscoelastic solids at the measured frequencies at fixed shear (ω = 1 rad s^{-1}, Figure 3a). A noticeable change in G' is observed as the chemical structure of the polymer backbone varies. With DMIZ as the organic base, the BPDA-mTB polymer backbone exhibits the strongest elastic response, followed by those of PMDA-mTB and 6FDA-mTB. An identical trend is observed in the results of the strain sweep measurements, with BPDA-mTB displaying a yield stress of 185.4 Pa, whereas those of PMDA-mTB and 6FDA-mTB are 38.4 and 19.3 Pa, respectively (Figure 3b). These results are presumably related to the interchain interactions between polymer chains. BPDA promotes interchain interactions, resulting in the enhancement of the mechanical robustness and modulus, whereas the bulky fluorinated functional group in 6FDA disrupts interchain interactions by a steric effect, thereby weakening the mechanical properties of polymer materials. Therefore, the interchain interactions between the polymer chains vary as the chemical structure changes, leading to differences in the elastic responses of the resulting HIPEs.

Variation in the organic base provides further diversity in the elastic response of the emulsion. The BPDA-mTB HIPEs are viscoelastic solids at internal volumes of 80 vol %, and G' decreases in the order of DMIZ, TEA, DMAP, and DMEA under the measurement conditions (Figure 3c). A change in the elastic response is observed during the strain sweep measurements. The yield strength of the HIPE with DMIZ is 185.4 Pa, which is considerably higher than those of the HIPEs

https://doi.org/10.1021/acsomega.3c09640
ACS Omega 2024, 9, 15222−15231

with TEA, DMAP, and DMEA (54.3, 40.4, and 28.5 Pa, respectively; Figure 3d). This variation in the elastic response is likely influenced by various factors, such as the hydrophobic−hydrophilic balance and viscosity of the aqueous PAAS solution. Therefore, the rheological study indicates that the design of the polymer backbone and its combination with an organic base should be considered in preparing a stable oil-in-water HIPE.

The structure fixation proceeded to obtain the continuous morphology from the HIPE template via freeze-drying. After freeze-drying at −40 °C for 24 h, white macroporous PAAS was obtained. The PAAS scaffold was converted to PI scaffold via thermal imidization by increasing the temperature to a maximum of 350 °C under vacuum (see Experimental Section for details), and thus, yellow sponge-like solids were obtained (Figure S8). The dimensions of the Macro PIs were almost intact compared with those of the macroporous PAASs, indicating that the thermal deformations of the polymers during the thermal process were negligible. The porosities of the resulting Macro PIs were determined by comparing their densities, and the porosities are shown in Table 1. All porous polymers display porosities of >99%, which are comparable to the theoretical porosities (99.4%) based on their compositions, indicating the presence of abundant pores within the polymer matrices.

The FT-IR spectra of the macroporous PAAS and Macro PI support the complete chemical conversion of the polymer scaffold from PAAS to PI (Figure S9). In the spectra of the macroporous PAASs, characteristic peaks representing the amide bonds are observed at 3000, 1643, and 1595 cm^{-1}. As the thermal process induces cyclization to form polyimide bonds, the peaks representing the amide are diminished. At the same time, peaks are observed at 1776, 1716, and 1358 cm^{-1}, corresponding to the C═O and C−N bonds of the imide. This spectral change appears to be the same regardless of the chemical structures of the polymer backbone and organic base. Additionally, peaks representing the tertiary amine are not observed, indicating that the organic bases are eliminated during the thermal imidization process.

The morphologies of the resulting Macro PIs were determined by using scanning electron microscopy (SEM), and the results are shown in Figure 4. The Macro PIs display bicontinuous, spherical porous structures, which are characteristic features of HIPE-derived porous polymers. These characteristic structures indicate that the HIPE prepared using PAAS polymers displays sufficient physical strength to withstand deformations during structural fixation and chemical conversion. The pore characteristics were also characterized with nitrogen adsorption analysis on the Macro PIs (Figure S10). For the macroporous PMDA-mTB, BPDA-mTB, and 6FDA-mTB, the nitrogen adsorption shows no capillary condensation profile at measuring conditions with the low BET surface (S_{BET}) in the range 11.8−29.2 $m^2\ g^{-1}$. This result corresponds well to the macroporous morphology observed by the SEM. Additionally, variations in the pore sizes are observed, depending on the chemical structure of the PAAS. The Macro PIs produced using the PAAS polymers conjugated with TEA and DMIZ exhibit relatively small pores and uniform pore size distributions (Figure 4 inset and Table 1), whereas the DMAP and DMEA series display larger pore diameters with wide pore size distributions. A change in the polymer backbone exhibits a lower correlation with the change in the pore size. These results indicate that organic bases significantly affect the stabilization of the emulsion interface to form small, stable internal droplets. In addition, the structural regularity is consistent with the results of the oscillatory measurements, which indicate that the polymers with DMIZ and TEA pendant groups exhibit enhanced interfacial activities. Therefore, the use of an appropriate organic base is critical in obtaining porous polymers with size-controlled pores using the emulsion template method.

The thermal and mechanical properties of the resulting Macro PIs were, respectively, confirmed using TGA and compression studies (Figures S11 and S12 and Table 1). The thermal stabilities of the resulting Macro PIs depend on their chemical structures. The BPDA-mTB series displays the highest average 5% decomposition temperature ($T_{d,5\%}$) of 519 °C, which is considerably higher than those of PMDA-mTB ($T_{d,5\%}$ = 504 °C) and 6FDA-mTB ($T_{d,5\%}$ = 467 °C). The thermal stabilities of polymers with the same backbone structures vary randomly, depending on their organic bases. This variation is presumably related to the completion of the reaction during thermal imidization and the change in the chain-packing structure of the polymer matrix, which should be addressed in future studies. Nevertheless, all compositions with the capacity to form Macro PIs with high porosities of >99% display outstanding thermal stabilities of >460 °C.

The stress−strain curves of the Macro PIs were obtained via compression studies (Figure S12). The elastic modulus (E) values of the Macro PIs were determined in the elastic region, and they are shown in Table 1. The mechanical properties of the resulting polymers vary according to their chemical structures and porous morphologies. On average, the BPDA-mTB series exhibits robust mechanical properties compared to those of the PMDA-mTB and 6FDA-mTB series, owing to the structural robustness of the polymer backbone. Additionally, porous polymers with regular pore size distributions exhibit higher E values, despite their identical chemical structures, e.g., BPDA-mTB/TEA and BPDA-mTB/DMIZ display respective moduli of 47.9 and 42.2 kPa, whereas those of BPDA-mTB/DMAP and BPDA-mTB/DMEA are 23.6 and 26.6 kPa, respectively. The 2-fold difference in E is presumably due to the porous morphologies of the resulting polymers, as observed in the SEM images (Figure 4). This trend is also observed in the PMDA-mTB series, suggesting that controlling the regularity of the porous morphology is crucial for producing high-performance functional polymers. However, the correlation between the porous morphology and mechanical properties of the 6FDA-mTB series is unclear because of the dense domains formed by pore collapse (Figure 4, last row). Based on the thermal and mechanical analyses of the Macro PIs, a porous polymer with a regular porous morphology displays the advantages of stronger mechanical and thermal properties. The dense structure with small pores exhibits a stronger resistance against changes in the external environment while maintaining its unique morphology. Therefore, developing a procedure for use in controlling the morphologies of highly porous materials is essential in preparing high-performance porous materials. In this respect, the development of a soft templating system using PAAS as the macrosurfactant is an effective approach for use in producing porous PI with a porosity of >99%.

The Macro PIs, which exhibit exceptional physical properties and overall porosities of >99%, were utilized as separators in rechargeable Li batteries. The porous structures of the Macro PIs should act as favorable pathways for Li-ion

https://doi.org/10.1021/acsomega.3c09640
ACS Omega 2024, 9, 15222−15231

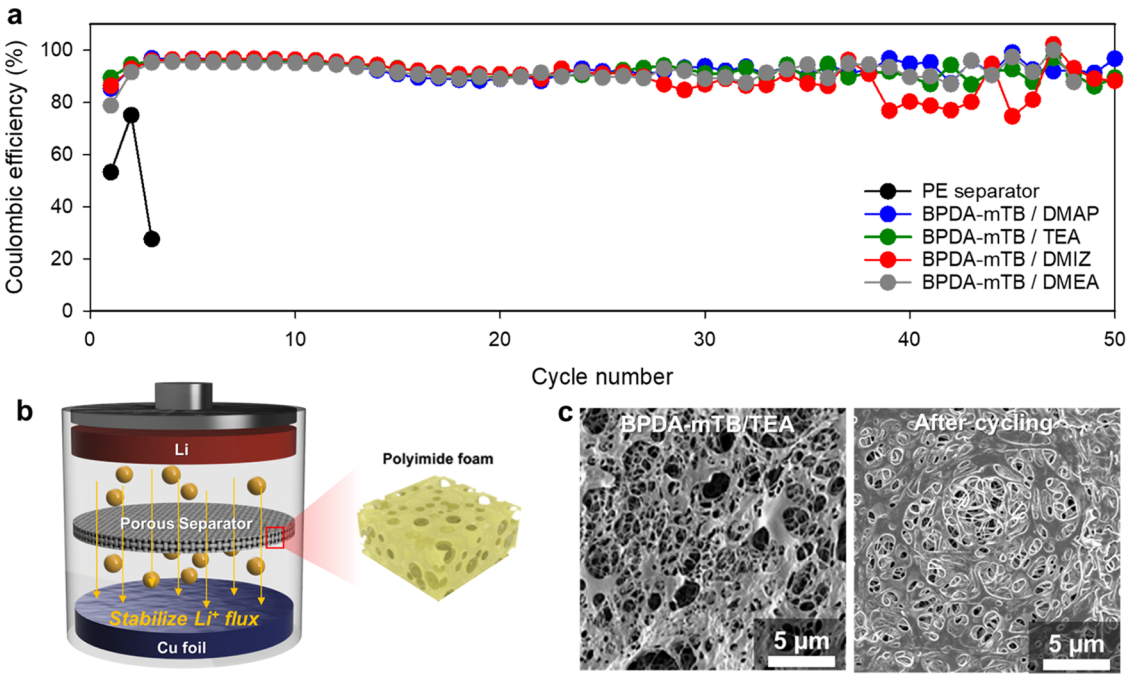

Figure 5. (a) Cyclic stabilities of Li/Cu cells with the as-prepared separators at a current density of 5.0 mA cm^{-2} and a capacity of 3.0 mAh cm^{-2}. (b) Schematics of a Li/Cu cell with the polyimide foam as a separator. (c) Scanning electron microscopy images of the BPDA-mTB/TEA separator before and after 50 cycles.

migration, thereby facilitating smooth Li-ion transport. The Macro PIs were applied as separators in Li-metal batteries, and their cyclic stabilities were evaluated using Li/Cu cells under harsh conditions with a high current density of 5.0 mA cm^{-2} and a capacity of 3.0 mAh cm^{-2} in a carbonate-based electrolyte. The results shown in Figure 5a reveal that a conventional polyethylene (PE) separator barely functions under these conditions, whereas the Macro PIs (BPDA-mTB/DMAP, BPDA-mTB/TEA, BPDA-mTB/DMIZ, and BPDA-mTB/DMEA) exhibit lifespans of >50 cycles with Coulombic efficiencies of >90%. The exceptional battery performance of the Macro PIs may be attributed to their capacities to stabilize the Li flux and facilitate rapid Li-ion migration, as shown in Figure 5b. The porous structures of the Macro PIs are crucial in these processes. To validate the stabilities of the separators, *ex situ* SEM imaging of the BPDA-mTB/TEA separator was performed after 50 cycles. Figure 5c shows that the porous structure remains intact, even after such demanding cycling, confirming the stabilities of the PI separators.

Our results provide compelling evidence that Macro PIs with excellent heat resistances and ultrahigh porosities are promising separators for use in Li-metal batteries. We foresee the possibility of applying these separators in various research areas to further enhance the development of advanced Li battery technologies.

CONCLUSIONS

We proposed the use of PAAS polymers as macrosurfactants in HIPEs. To verify the chemical structure dependence of the formation of a HIPE, 12 types of PAAS polymers were prepared in an aqueous solution. We formed 11 types of HIPEs at the water/toluene interface using the PAAS polymers as macrosurfactants. Rheological analysis suggested that emulsion stability was determined by the chemical structure of the polymer backbone and organic base, which is related to the hydrophilic−hydrophobic balance of the PAAS polymer. Additionally, HIPEs with sufficient mechanical strengths were necessary to prevent the deformation of porous structure during the freeze-drying and thermal imidization processes. The resulting Macro PIs displayed bicontinuous morphologies and micrometer-scale pores, with high porosities of >99%. The uniformities of the porous morphologies significantly affected the mechanical and thermal stabilities of the resulting porous polymers, even if the chemical structures of the polymer backbones were identical. Based on the observation of the porous materials, we demonstrated the use of Macro PIs as potential separators for use in Li-metal batteries. Our proposed process with PAAS as the macrosurfactant is an advanced method of preparing value-added PI materials.

ASSOCIATED CONTENT

Supporting Information

The Supporting Information is available free of charge at https://pubs.acs.org/doi/10.1021/acsomega.3c09640.

Additional synthetic scheme, NMR/FT-IR spectra, SEC trace, TGA thermogram, OM/visual image, BET data, and S−S curve. (PDF)

AUTHOR INFORMATION

Corresponding Authors

Mihye Wu − *Advanced Energy Materials Research Center, Korea Research Institute of Chemical Technology (KRICT), Daejeon 34114, Republic of Korea;* orcid.org/0000-0003-1068-906X; Email: wumihye@krict.re.kr

Yun Ho Kim − *Advanced Functional Polymers Center, Korea Research Institute of Chemical Technology (KRICT), Daejeon 34114, Republic of Korea; KRICT School, University of Science and Technology (UST), Daejeon 34113, Republic of Korea;* orcid.org/0000-0002-1722-5623; Email: yunho@krict.re.kr

https://doi.org/10.1021/acsomega.3c09640
ACS Omega 2024, 9, 15222−15231

Authors

Jongmin Park − *Advanced Functional Polymers Center, Korea Research Institute of Chemical Technology (KRICT), Daejeon 34114, Republic of Korea;* orcid.org/0000-0002-9112-6316

Sunkyu Kim − *Advanced Functional Polymers Center, Korea Research Institute of Chemical Technology (KRICT), Daejeon 34114, Republic of Korea; Department of Chemical Engineering, Hanyang University, Seoul 04763, Republic of Korea*

Jeonguk Hwang − *Advanced Functional Polymers Center, Korea Research Institute of Chemical Technology (KRICT), Daejeon 34114, Republic of Korea*

Jun Ha Choi − *Advanced Functional Polymers Center, Korea Research Institute of Chemical Technology (KRICT), Daejeon 34114, Republic of Korea; Department of Chemical and Biomolecular Engineering, Yonsei University, Seoul 03722, Republic of Korea*

Yujin So − *Advanced Functional Polymers Center, Korea Research Institute of Chemical Technology (KRICT), Daejeon 34114, Republic of Korea*

Sarang Park − *Advanced Functional Polymers Center, Korea Research Institute of Chemical Technology (KRICT), Daejeon 34114, Republic of Korea*

Min Jae Ko − *Department of Chemical Engineering, Hanyang University, Seoul 04763, Republic of Korea;* orcid.org/0000-0002-4842-3235

Jong Chan Won − *Advanced Functional Polymers Center, Korea Research Institute of Chemical Technology (KRICT), Daejeon 34114, Republic of Korea; KRICT School, University of Science and Technology (UST), Daejeon 34113, Republic of Korea;* orcid.org/0000-0003-3706-7359

Jungdon Suk − *KRICT School, University of Science and Technology (UST), Daejeon 34113, Republic of Korea; Advanced Energy Materials Research Center, Korea Research Institute of Chemical Technology (KRICT), Daejeon 34114, Republic of Korea*

Complete contact information is available at: https://pubs.acs.org/10.1021/acsomega.3c09640

Author Contributions

#J.P. and S.K. equally contributed.

Notes

The authors declare no competing financial interest.

■ ACKNOWLEDGMENTS

This study was supported by a KRICT Core Project (No. KS2321-20) and the National Research Foundation of Korea (NRF-2021R1A2C2006771 and NRF-2020M3H4A3081874).

■ REFERENCES

(1) Wu, D.; Xu, F.; Sun, B.; Fu, R.; He, H.; Matyjaszewski, K. Design and Preparation of Porous Polymer. *Chem. Rev.* **2012**, *112*, 3959−4015.

(2) Peters, E. C.; Svec, F.; Fréchet, J. M. J. Rigid Macroporous Polymer Monolith. *Adv. Mater.* **1999**, *14*, 1169−1181, DOI: 10.1002/(SICI)1521-4095(199910)11:143.0.CO;2-6.

(3) Gu, W.; Wang, G.; Zhou, M.; Zhang, T.; Ji, G. Polyimide-Based Foams: Fabrications and Multifunctional Applications. *ACS Appl. Mater. Interfaces* **2020**, *12*, 48246−48258.

(4) Shi, B.; Ma, B.; Wang, C.; He, H.; Qu, L.; Xu, B.; Chen, Y. Fabrication and Applications of Polyimide Nano-aerogels. *Composites, Part A* **2021**, *143*, 106283−106296.

(5) Ghaffari-Mosanezadeh, S.; Tafreshi, O. A.; Karamikamkar, S.; Saadatnia, Z.; Rad, E.; Meysami, M.; Naguib, H. E. Recent advances in tailoring and improving the properties of polyimide aerogels and their applications. *Adv. Colloid Interface Sci.* **2022**, *304*, 102646−102663.

(6) Guillen, G. R.; Pan, Y.; Li, M.; Hoek, E. M. V. Preparation and Characterization of Membranes Formed by Nonsolvent Induced Phase Separation: A Review. *Ind. Eng. Chem. Res.* **2011**, *50*, 3798−3817.

(7) Soroko, I.; Lopes, M. P.; Livingston, A. The effect of membrane formation parameters on performance of polyimide membranes for organic solvent nanofiltration (OSN): Part A. Effect of polymer/solvent/non-solvent system choice. *J. Membr. Sci.* **2011**, *381*, 152−162.

(8) Kim, M.; Kim, G.; Kim, J.; Lee, D.; Lee, S.; Kwon, J.; Han, H. New continuous process developed for synthesizing sponge-type polyimide membrane and its pore size control method via non-solvent induced phase separation (NIPS). *Microporous Mesoporous Mater.* **2017**, *242*, 166−172.

(9) Li, Y.; Xue, J.; Zhang, X.; Cao, B.; Li, P. Formation of macrovoid-free PMDA-MDA polyimide membranes using a gelation/non-solvent-induced phase separation method for organic solvent nanofiltration. *Ind. Eng. Chem. Res.* **2019**, *58*, 6712−6720.

(10) Xu, L.; Jiang, S.; Li, B.; Hou, W.; Li, G.; Memon, M. A.; Huang, Y.; Geng, J. Graphene oxide: a versatile agent for polyimide foams with improved foaming capability and enhanced flexibility. *Chem. Mater.* **2015**, *27*, 4358−4367.

(11) Yang, M.; Zhang, C.; Lv, Q.; Sun, G.; Bi, C.; Guo, S.; Dong, H.; Liu, L. Rational design of novel efficient palladium electrode embellished 3D hierarchical graphene/polyimide foam for hydrogen peroxide electroreduction. *ACS Appl. Mater. Interfaces* **2020**, *12*, 934−944.

(12) Cheng, Y.; Zhang, X.; Qin, Y.; Dong, P.; Yao, W.; Matz, J.; Ajayan, P. M.; Shen, J.; Ye, M. Super-elasticity at 4 K of covalently crosslinked polyimide aerogels with negative Poisson's ratio. *Nat. Commun.* **2021**, *12*, No. 4092.

(13) Zheng, S.; Jiang, L.; Zhang, C.; Ma, N.; Liu, X. Facile and environment-friendly preparation of high-performance polyimide aerogels using water as the only solvent. *Polym. Chem.* **2022**, *13*, 2375−2382.

(14) Kimmins, S. D.; Carmeron, N. R. Functional porous polymers by emulsion templating: Recent advances. *Adv. Funct. Mater.* **2011**, *21*, 211−225.

(15) Pulko, I.; Krajnc, P. High internal phase emulsion templating-a path to hierarchically porous functional polymers. *Macromol. Rapid Commun.* **2012**, *33*, 1731−1746.

(16) Silverstein, M. S. PolyHIPEs: Recent advances in emulsion-templated porous polymers. *Prog. Polym. Sci.* **2014**, *39*, 190−234.

(17) Zhang, T.; Sanguramath, R. A.; Israel, S.; Silverstein, M. S. Emulsion templating: porous polymers and beyond. *Macromolecules* **2019**, *52*, 5445−5479.

(18) Teo, N.; Gu, Z.; Jana, S. C. Polyimide-based aerogel foams, via emulsion-templating. *Polymer* **2018**, *157*, 95−102.

(19) Male, U.; Huh, D. S. Fabrication of Robust honeycomb patterned porous films by thermochemical cross-linking of polyimide. *Polymer* **2019**, *178*, 121597−121602.

(20) Ghosh, M. K.; Mittal, K. L. *Polyimide: Fundamentals and Applications*; Marcel Dekker Inc., 1996.

(21) Liaw, D.-J.; Wang, K.-L.; Huang, Y.-C.; Lee, K.-R.; Lai, J.-Y.; Ha, C.-S. Advanced polyimide materials: Syntheses, physical properties, and applications. *Prog. Polym. Sci.* **2012**, *37*, 907−974.

(22) Lu, Z.; Sui, F.; Miao, Y.-E.; Liu, G.; Li, C.; Dong, W.; Cui, J.; Liu, T.; Wu, J.; Yang, C. Polyimide separators for rechargeable batteries. *J. Energy Chem.* **2021**, *58*, 170−197.

(23) Nagasaki, M.; Kanamura, K. High-performance lithium metal rechargeable battery using an ultrafine porous polyimide separator

with three-dimensionally ordered macroporous structure. *ACS Appl. Energy Mater.* **2019**, *2*, 3896−3903.
(24) Wang, H.; Wang, T.; Yang, S.; Fan, L. Preparation of thermal stable porous polyimide membranes by phase inversion process for lithium-ion battery. *Polymer* **2013**, *54*, 6339−6348.
(25) Meador, M. A. B.; Wright, S.; Sandberg, A.; Nguyen, B. N.; Van Keuls, F. W.; Mueller, C. H.; Rodríguez-Solís, R.; Miranda, F. A. Low dielectric polyimide aerogels as substrates for lightweight patch antennas. *ACS Appl. Mater. Interfaces* **2012**, *4*, 6346−6353.
(26) Hou, X.; Mao, Y.; Zhang, R.; Fang, D. Super-flexible polyimide nanofiber cross-linked polyimide aerogel membranes for high efficient flexible thermal protection. *Chem. Eng. J.* **2021**, *417*, 129341−129348.
(27) Zheng, S.; Jiang, L.; Chang, F.; Zhang, C.; Ma, N.; Liu, X. Mechanically Strong and Thermally Stable Chemical Cross-Linked Polyimide Aerogels for Thermal Insulator. *ACS Appl. Mater. Interfaces* **2022**, *14*, 50129−50141.
(28) Ma, J.; Zhan, M.; Wang, K. Ultralightweight Silver Nanowires Hybrid Polyimide Composite Foams for High-Performance Electromagnetic Interference Shielding. *ACS Appl. Mater. Interfaces* **2015**, *7*, 563−576.
(29) Wang, Y.-Y.; Zhou, Z.-H.; Zhou, C.-G.; Sun, W.-J.; Gao, J.-F.; Dai, K.; Yan, D.-X.; Li, Z.-M. Lightweight and Robust Carbon Nanotube/Polyimide Foam for Efficient and Heat-Resistant Electromagnetic Interference Shielding and Microwave Absorption. *ACS Appl. Mater. Interfaces* **2020**, *12*, 8704−8712.
(30) Zembyla, M.; Murray, B. S.; Sarkar, A. Water-in-oil emulsions stabilized by surfactants, biopolymers and/or particles: a review. *Trends Food Sci. Technol.* **2020**, *104*, 49−59.
(31) Brown, J. F.; Krajnc, P.; Cameron, N. R. PolyHIPE supports in batch and flow-through Suzuki cross-coupling reactions. *Ind. Eng. Chem. Res.* **2005**, *44*, 8565−8572.
(32) Kovačič, S.; Štefanec, D.; Krajnc, P. Highly porous open-cellular monoliths from 2-hydroxyethyl methacrylate based high internal phase emulsions (HIPEs): preparation and void size tuning. *Macromolecules* **2007**, *40*, 8056−8060.
(33) Kim, K.; Kim, S.; Ryu, J.; Jeon, J.; Jang, S. G.; Kim, H.; Gweon, D.-G.; Im, W. B.; Han, Y.; Kim, H.; Chio, S. Q. Processable high internal phase Pickering emulsions using depletion attraction. *Nat. Commun.* **2017**, *8*, No. 14305.
(34) Durgut, E.; Sherborne, C.; Dikici, B. A.; Reilly, G. C.; Claeyssens, F. Preparation of interconnected Pickering polymerized high internal phase emulsions by arrested coalescence. *Langmuir* **2022**, *38*, 10953−10962.
(35) Cai, R.; You, Y.; Wu, P.; Liu, Q.; Zhu, Y.; Zhang, S. Preparation of Open-Cell Rigid Polyimide Foam via Nonaqueous High Internal Phase Emulsion-Templating Technique. *ACS Appl. Polym. Mater.* **2023**, *5*, 7795−7804.
(36) Williams, J. M.; Wrobleski, D. A. Spatial distribution of the phases in water-in-oil emulsion. Open and closed microcellular foam from cross-linked polystyrene. *Langmuir* **1988**, *4*, 656−662.
(37) Wu, R.; Menner, A.; Bismarck, A. Macroporous polymers made from medium internal phase emulsion templates: Effects of emulsion formulation on the pore structure of polyMIPEs. *Polymer* **2023**, *54*, 5511−5517, DOI: 10.1016/j.polymer.2013.08.029.
(38) Kim, M.; Yang, K.; Kim, Y. S.; Won, J. C.; Kang, P.; Kim, Y. H.; Kim, B. G. Laser-induced photothermal generation of flexible and salt-resistant monolithic bilayer membranes for efficient solar desalination. *Carbon* **2020**, *164*, 349−356.
(39) Choi, J.; Yang, K.; Bae, H-.S.; Phiri, I.; Ahn, H. J.; Won, J. C.; Lee, Y. M.; Kim, Y. H.; Ryou, M.-H. Highly stable porous polyimide sponge as a separator for lithium-metal secondary batteries. *Nanomaterials* **2020**, *10*, 1976−1992.
(40) Facinelli, J. V.; Gardner, S. L.; Dong, L.; Sensenich, C. L.; Davis, R. M.; Riffle, J. S. Controlled Molecular Weight Polyimides from Poly(amic acid) Salt Precursors. *Macromolecules* **1996**, *29*, 7342−7350.
(41) Cao, Z.; Zhao, X.; Wang, D.; Chen, C.; Qu, C.; Liu, C.; Hou, X.; Li, L.; Zhu, G. Polymerization of poly-(amic acid) ammonium salt in aqueous solution and its use in flexible printed circuit boards. *Eur. Polym. J.* **2017**, *96*, 393−402.
(42) Jeong, Y.; Park, H.; So, Y.; Mun, H. K.; Shin, T. J.; Park, N. K.; Kim, J.; Yoo, S.; Won, J. C.; Kim, Y. H. Enhanced hydrolytic and electrical stability of eco-friendly processed polyimide gate dielectrics for organic transistors. *J. Mater. Chem. C* **2020**, *8*, 14370−14377.
(43) Lee, H.; Kim, D.; Kim, S. H.; So, Y.; Kim, Y. H.; Kim, J.; Park, J.; Cho, J. H.; Won, J. C. A water-borne photo-sensitive polyimide precursor for an eco-friendly process of preparing organic thin film transistors. *J. Mater. Chem. C* **2023**, *11*, 3459−3467.
(44) Cai, D.; Su, J.; Huang, M.; Liu, Y.; Wang, J.; Dai, L. Synthesis, characterization and hydrolytic stability of poly(amic acid) ammonium salt. *Polym. Degrad. Stab.* **2011**, *96*, 2174−2180.
(45) Brunauer, S.; Emmett, P. H.; Teller, E. Adsorption of gases in multimolecular layers. *J. Am. Chem. Soc.* **1938**, *60*, 309−319.

https://doi.org/10.1021/acsomega.3c09640
ACS Omega 2024, 9, 15222−15231